The Astronomical Journal, 154:276 (11pp), 2017 December https://doi.org/10.3847/1538-3881/aa9565

Observational Study of an Unusual Cataclysmic Binary 2MASS J16211735+4412541*

S. Zola[1,2], P. Szkody[3], S. Ciprini[4,5], F. Verrecchia[4,6], B. Debski[1], W. Ogloza[2], M. Drozdz[2], D. Reichart[7], D. B. Caton[8], and V. L. Hoette[9]
[1] Astronomical Observatory, Jagiellonian University, ul. Orla 171, PL-30-244 Krakow, Poland; szola@oa.uj.edu.pl
[2] Mt. Suhora Observatory, Pedagogical University, ul. Podchorazych 2, PL-30-084 Krakow, Poland
[3] Department of Astronomy, University of Washington, Box 351580, Seattle, WA 98195, USA
[4] Space Science Data Center—Agenzia Spaziale Italiana, via del Politecnico, snc, I-00133, Roma, Italy
[5] Instituto Nazionale di Fisica Nucleare, Sezione di Perugia, Perugia I-06123, Italy
[6] INAF Osservatorio Astronomico di Roma, via Frascati 33, I-00040 Monteporzio Catone, Italy
[7] University of North Carolina at Chapel Hill, Chapel Hill, NC 27599, USA
[8] Dark Sky Observatory, Department of Physics and Astronomy, Appalachian State University, Boone, NC 28608, USA
[9] Yerkes Observatory, Department of Astronomy and Astrophysics, University of Chicago, 373 W. Geneva Street, Williams Bay, WI 53191, USA
Received 2017 July 29; revised 2017 October 3; accepted 2017 October 21; published 2017 December 4

Abstract

We present results from an observational campaign on the close binary system 2MASS J16211735+4412541 and a preliminary model based on the photometric data gathered during the quiescent and outburst levels. The modeling, done with the Wilson–Devinney code and its improvements, failed to reproduce the observational properties of the system. A secondary minimum obtained within the stellar model that is too shallow, as well as the evidence provided by the spectroscopic observations performed at outburst and quiescence, point toward an accretion disk surrounding one component, likely a white dwarf, as the cause of the outburst. Using a simple disk model, we modeled the observed multicolor light curves taken two (2016 August) and eight (2017 March) months after the outburst. We obtained a reasonable fit to the 2016 August light curves but those from 2017 March cannot be explained with the same parameters. We conclude that J1621 is an eclipsing cataclysmic binary, with an accretion disk still present almost a year after outburst, and not a contact-type system as previously classified. The binary is seen at an inclination of about 84° and there is evidence of changing accretion rates and disk parameters as a result of the outburst. Our results indicate that more cataclysmic variables may be hidden among contact binaries.

Key words: binaries: eclipsing – novae, cataclysmic variables – stars: dwarf novae – stars: individual (2MASS J16211735+4412541) – ultraviolet: stars

1. Introduction

In recent years, large sky surveys have announced copious discoveries of short-period binary stars. In those surveys, binaries are generally divided into three categories based on the shape of their light curves. This classification process usually identifies the EA-type light curve with a detached system, the EB-type light curve with a semi-detached system and the EW-type light curve with a contact binary star. In the Catalina Real-Time Transient Survey (Drake et al. 2014b, hereafter CRTS), about 50% of all binaries are assigned to the family of contact binaries. Although such classified objects agree with the color–color and color–period relations for (near) contact binaries in general, many of them may prove not to be contact binaries at all. Drake et al. (2014a) pointed out that there could be a considerable fraction of binaries in CRTS consisting of a white dwarf and a late-type main-sequence star with light curves typical of the EW-type. It would be next to impossible to distinguish them from genuine contact binaries without a spectroscopic case study, as both types may have similar colors, especially if the white dwarf in the WD+dM binary has a low surface temperature and/or is totally or partly hidden in an accretion disk. Such noneclipsing WD+dM binaries with a cool white dwarf could successfully mimic classical contact binary systems and even modeling of their photometric light curves may lead to a conclusion that a system has a contact configuration (Zola 1995, 1998).

CSS J162117.4+441254 (2MASS J16211735+4412541, SDSS J162117.35+441254.1, J1621 hereafter) upon discovery (Lohr et al. 2013; Palaversa et al. 2013; Drake et al. 2014b) was classified as a contact binary with an orbital period of 0.2087521 days. The mean brightness of the system was $u = 17.54$, $g = 15.76$, $r = 14.92$, $i = 14.56$, $z = 14.37$ (SDSS, York et al. 2000); FUV = 20.5, NUV = 20.2 (*GALEX*, Martin et al. 2005). Drake et al. (2016) reported its unexpected brightening on 2016 June 4th. Due to the possibility that the brightening might have been the first stage of a rare, V1309 Scorpii-type merger resulting in a red nova event (Tylenda et al. 2011), a number of observers answered the call for further observations (e.g., Zejda & Pejcha 2016). According to Maehara (2016) the system was already in outburst on 2016-06-01.61598 UT reaching 12.19 Ic-band magnitude.

Results from quiescent photometric observations of J1621 taken in 2016 June 2 weeks after outburst, have been reported by Kjurkchieva et al. (2017). They also summarized archival (AAVSO, SWASP) light curves along with their new photometric observations of this system. The basic properties of the light-curve evolution were described and a preliminary model for the system both in the outburst and the quiescent states proposed. According to their results, the system consists of a cool (4700 K) dwarf filling its Roche lobe and a cool (4400 K) white dwarf. During the outburst, the white dwarf is

* Based on observations obtained with the Apache Point Observatory (APO) 3.5 m telescope, which is owned and operated by the Astrophysical Research Consortium (ARC).

surrounded by an accretion disk formed from the matter transferred through the Lagrangian L_1 point from the main-sequence secondary. The system rise in brightness is due to the light contribution from the disk. Within the proposed model, during quiescence the system consists of the bare stars with a hot spot on the white dwarf and a cool spot on the secondary.

2. Observations

2.1. Photometry

The outburst of J1621 was spotted at the very beginning of 2016 June . We gathered multicolor photometric data covering nights from June 4th up to the first week of 2016 September. During the next observing season, in 2017 March, a complete light curve in BVRI was also collected. In 2016, we observed the entire outburst after it was reported, with only one missing night: June 9/10. The photometry covering full orbital periods was conducted with Polish telescopes in Krakow (TEL50), Mt. Suhora (SUH), the Skynet DSO-14/17, and Yerkes-41 robotic telescopes. The Yerkes-41 telescope data were obtained with the Sloan *griz* filters and the Hα filter. Other telescopes were equipped with sets of wide band filters and observations were mostly taken with the R filter. When the system returned to its low state, we performed observations at Mt. Suhora observatory with the 60 cm telescope aimed at getting a multicolor light curve in BVRI filters. The evolution of brightness in the R filter is shown in Figure 1 (top panel), while the bottom panel of this figure shows how the shape of the light curve in the V filter was changing over several nights during the outburst. Note the depth decrease of the V-shaped minimum from June 8 to 12. The width and the shape of the minimum also evolved as the outburst progressed. We define the deep minimum at outburst as the primary minimum and establish its phase as zero. Note that this is different from the past light curves at quiescence, which have defined the primary minimum as the deeper minimum during that time, which occurs at our phase 0.5.

The outburst ended between June 10 and 12 (due to bad weather, we have no complete light curve for June 11th). Within a week, the luminosity of J1621 decreased by about 1.5 mag in the R filter. During the outburst, the light curve showed a 0.9 mag deep (Johnson R band) V-shaped minimum corresponding to the secondary eclipse from the CRTS archival data. With time, both its depth and width decreased and within a week reached the properties typical of the low state. The deep V-shaped minimum became hardly visible on June 12/13 (see the bottom right panel in Figure 2). The secondary minimum, which was much shallower during the outburst, became considerably deeper than the primary just after the outburst ended. The post-outburst shape of the light curve looks similar to the one from the CRTS archive, although in June the amplitude of the variations was larger in comparison to the pre-outburst data. In July, the light curve started to flatten toward the pre-outburst amplitude and the target had a similar shaped light curve in 2016 August. When the new observing season started, we took one more set of multicolor light curves of J1621 in 2017 March. After J1621 returned to its low state, its brightness stayed at roughly the same level, and the shape of the light curve did not change much. It looked very similar in 2016, July, and August. However, during observations taken in 2017 March, about eight months after the outburst, some change can be noted. The shape is still dominated by the ellipsoidal effects but the difference of the maxima heights is not as pronounced as in 2016, being almost negligible. Even after that period, the light curve does not look quite like that of a typical contact system. Shallow minima at phase 0 are still present and their depth increases toward shorter wavelengths. This means that the variability the system exhibits is a combination of a dominant ellipsoidal effect caused by a K-type component and shallow eclipses due to obscuration of a significantly hotter companion by the K star. Except for the geometrical effect, there is also an intrinsic variability present in the low state, clearly seen in shorter wavelengths (see the bottom right panel of Figure 3). It resembles irregular, fast light changes typical of flickering observed in cataclysmic binaries and originating in the disk surrounding the primary component. Observations spanning the period of about 8 months after the outburst show no significant change of the J1621 brightness level, but intrinsic variability was present in the form of flickering as noted above and asymmetries in its optical light curve were still evident.

On five nights, we took data with the Yerkes-41 telescope through the Hα filter. The results are presented in Figure 4. The left panel shows all data while the right panel has the same data but with the phases of the observations. On June 7 (JD 2457546.8), when the outburst was already in progress, we caught a rapid increase of brightness in Hα. In less than 20 minutes, there was a small decrease, followed by a jump in brightness of J1621 by about 0.5 mag. The difference between the comparison and check stars remained constant. On the next night, J1621 was even brighter, about 1.1 mag above its post-outburst level. The phase of the June 7th data (phase 0) implies the variability in Hα is likely to be the result of obscuration of the primary by the secondary component, as this short run happened to occur exactly during the primary minimum. Our observations during the quiescent state also revealed intrinsic variability in Hα.

2.2. Spectroscopy

Spectra of J1621 at outburst were obtained on 2016 June 4/5 and at quiescence on 2017 June 22/23 with the Double Imaging Spectrograph on the 3.5 m telescope at the Apache Point Observatory. This instrument obtains simultaneous blue and red spectra in two channels. The high-resolution gratings (1200) were used in each channel, providing wavelength coverage from 4000 to 5000 Å in the blue and 6000–7200 Å in the red with spectral resolution of 0.6 Å pixel^{-1}. At outburst, eight spectra were obtained, and one spectrum at quiescence using a 1.5 arcsec slit in partially cloudy conditions with the seeing about 2 arcsec. The exposures were 10 minutes for all, with the total time for the eight outburst spectra spanning from 3:27 to 6:00 UT 2016 June 5 and the single exposure centered at 6:25 UT 2017 June 23. Calibration lamps and flux standards were obtained and IRAF tasks were used to extract the spectra and convert them to wavelength and flux. The centroid "e" routine in the splot package was used to measure the line centers, equivalent widths and fluxes of the emission lines in each spectrum. Sections of the resulting outburst spectra are presented in Figure 5, and a comparison of the full spectra at the same phase (0.9) at outburst and quiescence is shown in Figure 6.

The 2016 June spectra were obtained at the peak of outburst, 4 days after the outburst rise (Maehara 2016, vsnet-alert 19861). All 8 spectra show the Balmer lines in emission and

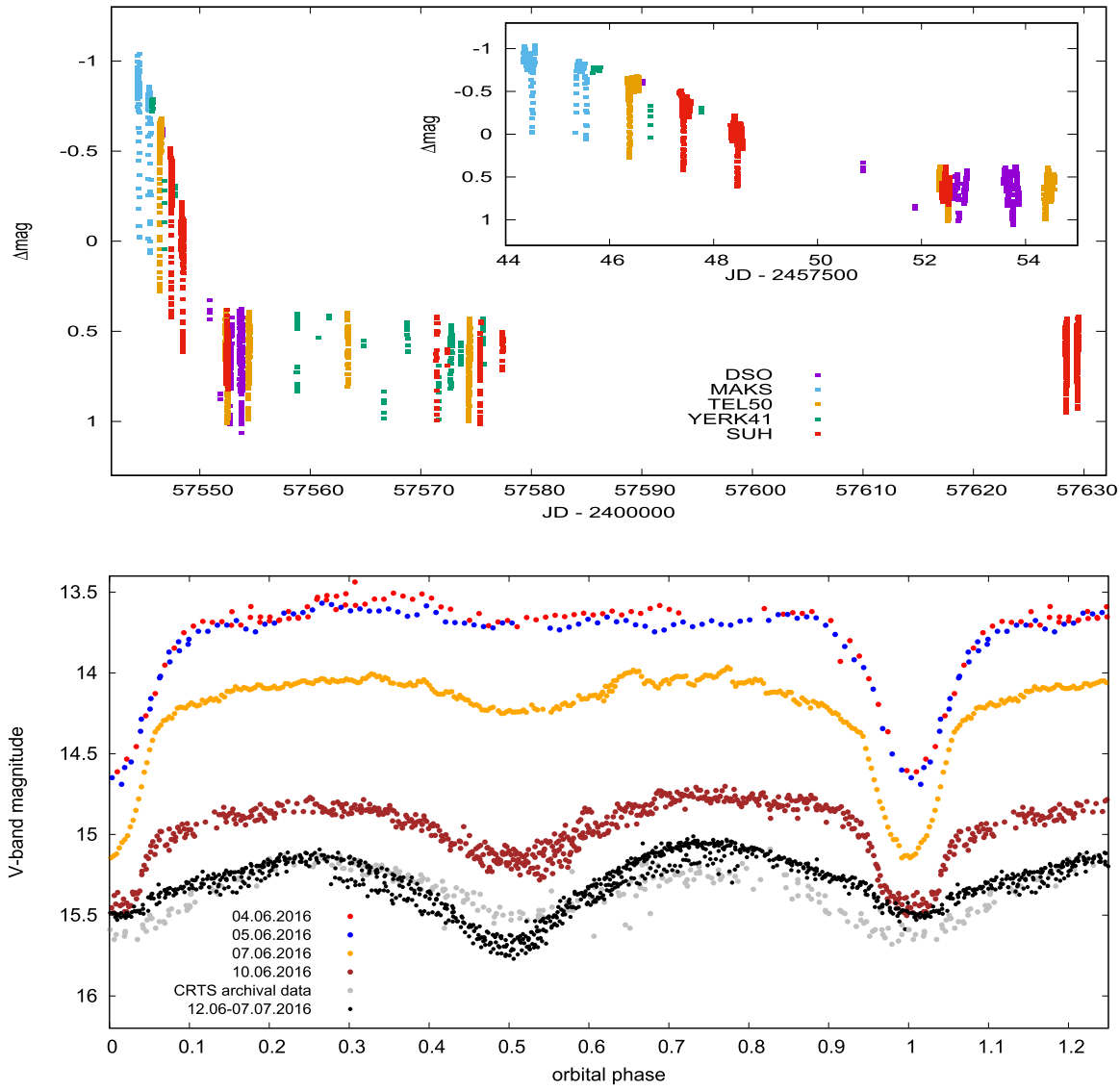

Figure 1. Brighness change of J1621 in the R filter against the comparison star (top panel). The zoom around the outburst is shown in the inset window. The evolution of the light-curve shape in the V filter is shown in the bottom panel.

the He II4686 high excitation emission line stronger than Hβ (Figure 5). The equivalent widths of He II, Hβ, and Hα, measured at phase 0.13, are 38, 19, and 37 Å respectively. Since most dwarf novae at outburst usually have broad Balmer absorption lines with weak emission cores and only some weak evidence of He II (Warner 1995), the strength of the emission lines in these spectra is unusual. The spectra are similar to the high inclination dwarf nova IP Peg at outburst (Piche & Szkody 1989; Marsh & Horne 1990). In that object, Marsh & Horne attributed the strong emission lines partly to an inclined disk, which could suppress the continuum relative to the emission lines. The inclination of IP Peg (81°) is similar to that of J1621. The doubled Balmer lines that are most visible at phases 0.90 and 0.13 in Figure 5, are the typical signature of an accretion disk and prove that an accretion disk is present. This doubling provides one of the strongest arguments that this system is not a contact binary. In addition, a strong rotational disturbance attributed to the eclipse of a disk is evident at phases 0.97 and 0.01 when the lines shift sharply from red to blue. Transforming the line centers to velocities shows a velocity shift from +250 km s^{-1} at phase 0.97 to −350 km s^{-1} at phase 0.01 in the Hβ line. Fitting the remaining 6 velocity points at other phases for each line to a sine wave with the period fixed at 5 hr produces radial velocity curves with K semi-amplitudes of 176 ± 32 km s^{-1} for Hα, 183 ± 38 km s^{-1} for Hβ, and 74 ± 2 km s^{-1} for He II. These values can be compared to the 115 ± 6 km s^{-1} determined for the Balmer emission lines from a full orbit data set when J1621 had returned to quiescence on June 11 (Thorstensen 2016). The differences show that He II comes from a different location than the Balmer lines and that the accretion disk likely has a different shape at outburst than at quiescence.

Like IP Peg, the Hβ and Hα lines in J1621 show a narrow component superposed on the broad emission that moves from blue to red, which is a typical signature of a hot spot (Figure 5). The blue component is very visible at phase 0.7 and the red component is becoming visible at phase 0.13. An interesting feature of the He II line is the narrow central component at phase 0.90. This could be related to the stationary component seen in IP Peg and interpreted as a wind component (Piche & Szkody 1989; Marsh & Horne 1990) or slingshot prominences (Steeghs et al. 1996). The comparison of the outburst spectra to

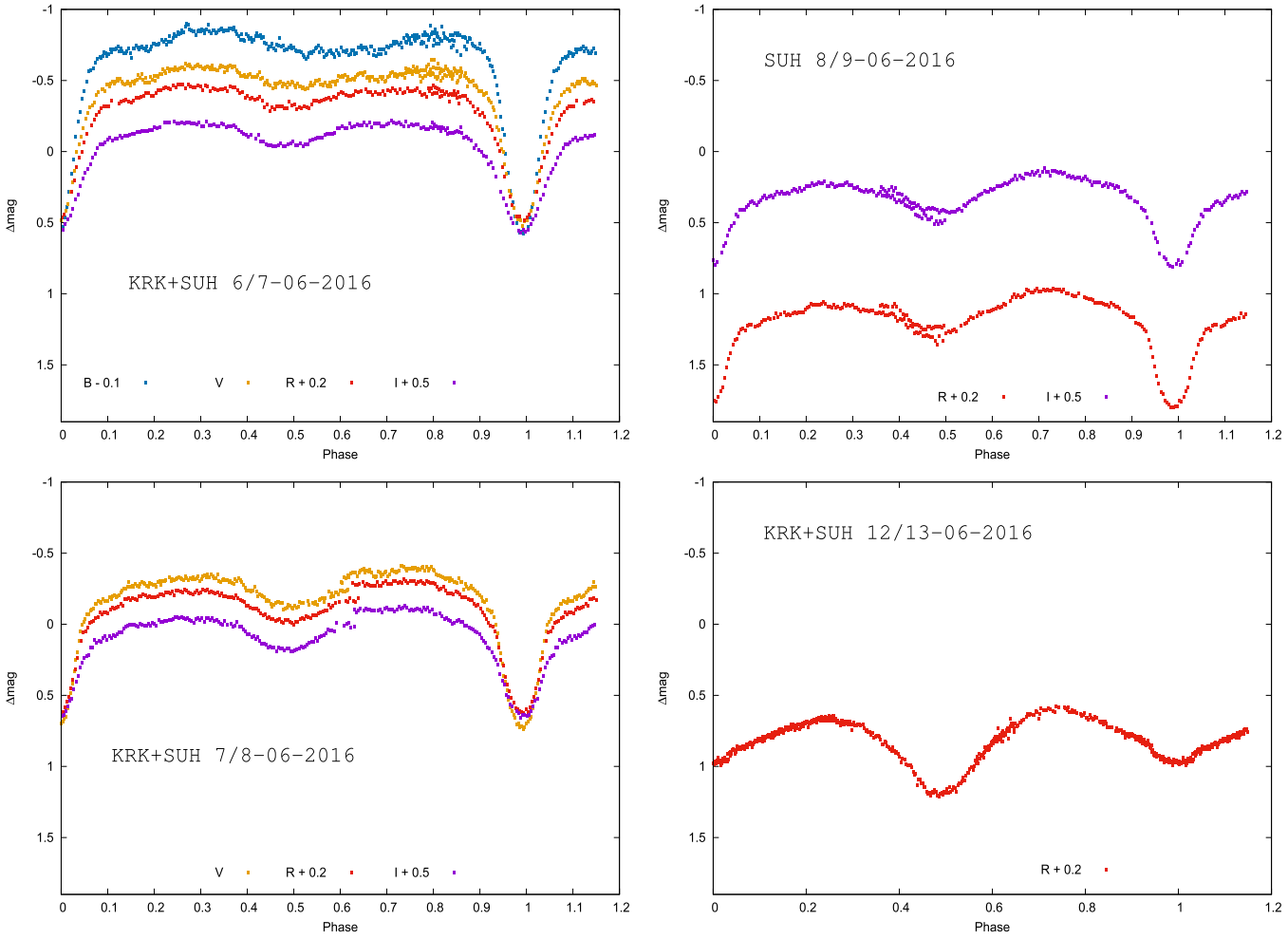

Figure 2. Multicolor light curves of J1621 at outburst. The scale of each panel is the same to show the decline in brightness and changing shape of the light curve. Δmag denotes the magnitude difference between J1621 and the comparison star (3UC269-134839).

the spectrum obtained one year later during quiescence (Figure 6) shows several notable contrasts. The blue continuum fluxes are an order of magnitude larger during outburst than quiescence. The continuum shape changes as the quiescent data show the upturn caused by the increased contribution of the K secondary to the total light. The strength of the He II4686 line changes from larger than Hβ at outburst to nondetection at quiescence. The full width zero intensity of the Hα and Hβ lines are 8–9 Å larger during outburst than quiescence. All of these changes are consistent with an increased disk contribution at outburst than at quiescence, as is typical of dwarf novae.

2.3. *Swift* X-Ray and UV Observations

A dedicated follow-up ToO observing program using the *Swift* satellite of J1621 was performed on 2016 June 10 and 14 when the binary star was already at quiescence. The *Swift* observations were performed using two of three on-board instruments: the X-ray Telescope (XRT; Burrows et al. 2005, 0.2–10.0 keV) and the UltraViolet Optical Telescope (UVOT; Roming et al. 2005, 170–600 nm). The XRT data for these observations were taken in Photon Counting mode. The *Swift* satellite observed J1621 six times (with a further four observations taken in Window Timing mode on 2017 January 10, 13, 16, and 19) for a total exposure of 5700 s. The analysis of the summed event data from all six observations resulted in a positive detection of the cataclysmic binary star J1621 in the soft X-ray band with a faint flux. The XRT data set was first reprocessed with standard procedures (`xrtpipeline`) for calibration and cleaning, and treated with filtering and screening criteria by using the `Heasoft` package (v6.21). The accumulated energy spectrum of the source summing and combining all six observations was extracted taking source events from a circular region with a radius of 20 pixels centered on the J1621 position, while background events were extracted from a circular region with a radius of 50 pixels, away from background sources. Since the source count rate was low, no pile-up correction was necessary. Ancillary response files were generated with `xrtmkarf`, and account for different extraction regions, vignetting and PSF corrections. The individual XRT X-ray energy spectrum accumulated from all the observations is rebinned with a minimum of one count per energy bin to allow W-statistic fitting within `XSPEC`, automatically selected in case of Poisson source counts with Poisson background. In the limit of large numbers of counts per spectrum energy bin, a second-order Taylor expansion shows that the W statistic tends to a sum distributed as χ^2. The summed individual spectrum is fitted with a simple absorbed power law, with a neutral hydrogen-equivalent column density

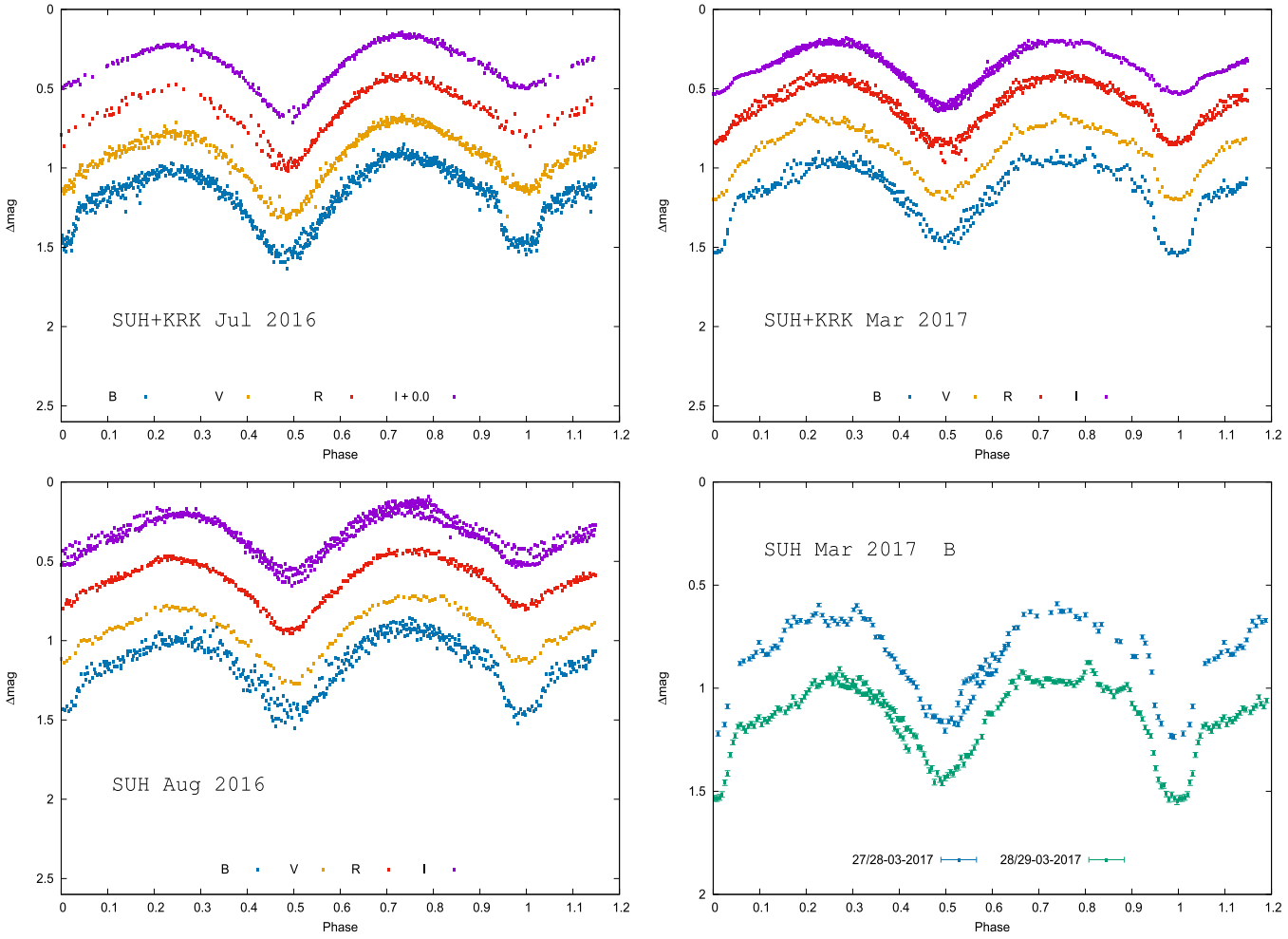

Figure 3. Multicolor light curves of J1621 taken in 2016 July and August, and in 2017 March. A light curve gathered in the B filter, showing intrinsic variability, is presented in the bottom right panel.

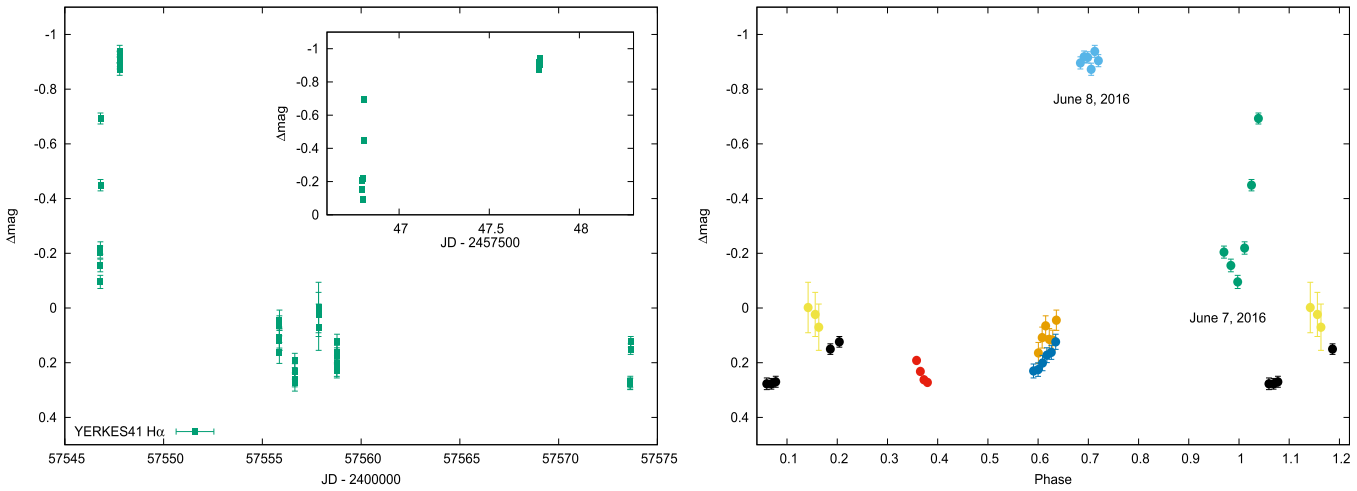

Figure 4. Brighness variations of J1621 in the H_α filter. All data we gathered are presented in the left panel. The inset window shows observations taken at outburst. The right panel shows H_α filter observations phased with the ephemeris listed in Section 3.1 with data taken on June 7 and 8 labeled. Data taken at different nights are plotted with a different color.

fixed to its Galactic value along the line of sight of 1.6×10^{21} cm^{-2} (Kalberla et al. 2005). The resulting unabsorbed 0.3–10 keV flux for all the accumulated observations is $(2.2^{+5.0}_{-0.8}) \times 10^{-13}$ erg cm^{-2} s^{-1} and the corresponding photon spectral index is 1.9 ± 1.2. We checked the source detection on the summed XRT event data using the Ximage (within HEASoft) "sosta" routine, which takes into account the PSF, exposure, and vignetting, to estimate source count rate and

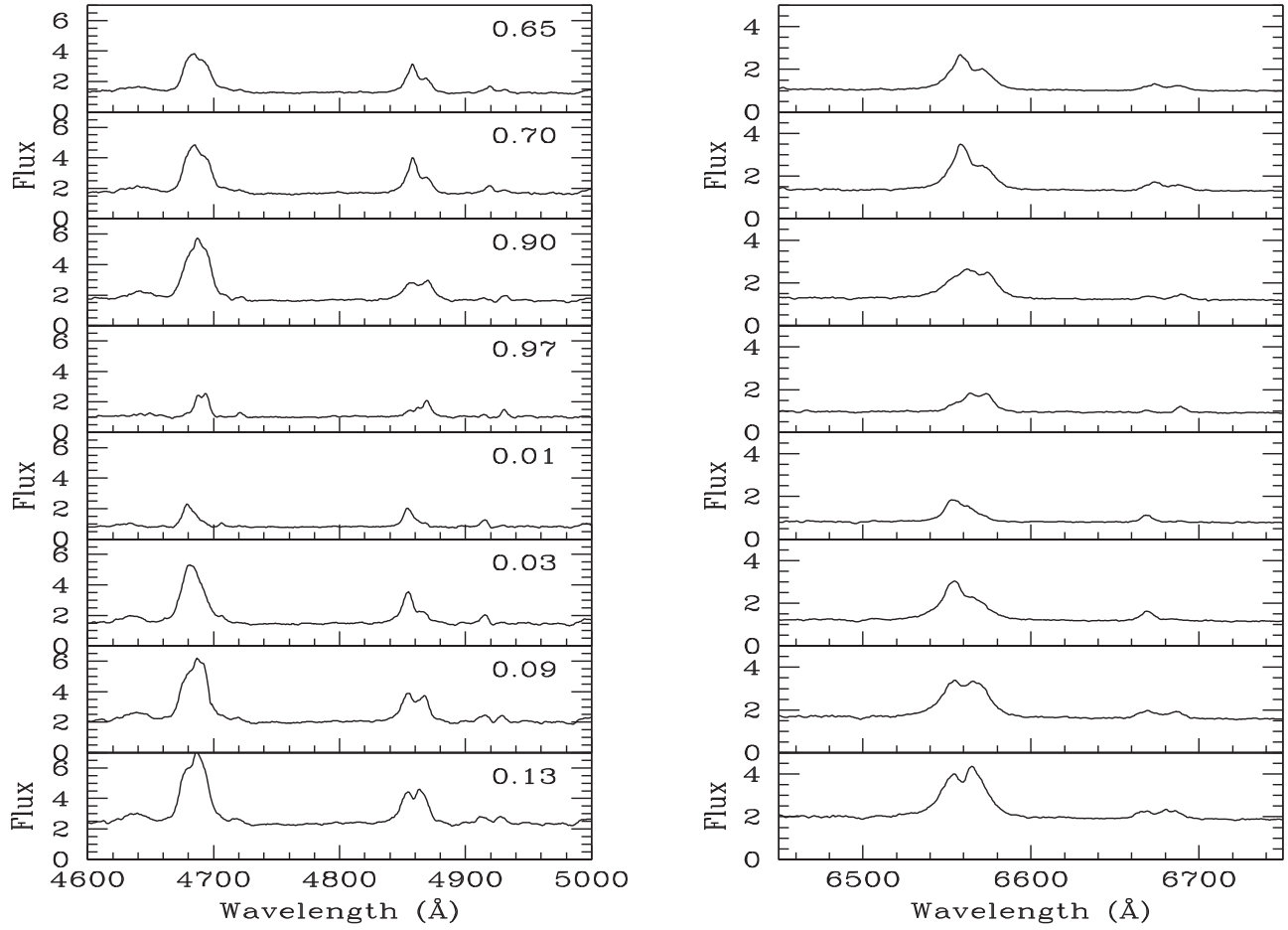

Figure 5. Sequence of spectra of He II and Hβ (left) and Hα (right) obtained on 2016 June 5 at peak of outburst. The fluxes are in units of 10^{-14} erg cm^{-2} s^{-1}Å^{-1}. Phases are marked in the upper right of the left plots.

signal-to-noise ratio (S/N). We obtained an S/N of 4.6 in the full band.

The *Swift* UVOT telescope (Roming et al. 2005) can acquire images in six lenticular filters (V, B, U, W1, M2, and W2, with central wavelengths in the range of 170–600 nm; Breeveld et al. 2011). After 12.5 years of operations, observations are now carried out using only one of the filters unless specifically requested by the user. Simultaneous to XRT, UVOT observations of J1621 were requested and obtained using all the optical and UV filters. The log and photometric results of UVOT observations analyzed are reported in Table 1.

The photometric analysis of all six observations were performed using the standard UVOT software distributed within the `HEASoft` 6.16 package and the calibration included in the most recent release of the "Calibration Database." We extracted source counts using a standard circular aperture with a 5″ radius for all filters, and the background counts using three circular apertures with 18″ radii. Source counts were converted to fluxes using the task `uvotsource` and the standard zero points (Breeveld et al. 2011). Fluxes were then dereddened using the appropriate extinction factor value $E(B-V) = 0.00908$ for the source position according to Schlegel et al. (1998) and Schlafly & Finkbeiner (2011) and the $A_\lambda/E(B-V)$ ratios were calculated for UVOT filters using the mean Galactic interstellar extinction curve from Fitzpatrick (1999). Source magnitudes from aperture photometry for each complete exposure image frame are also calculated, and the dereddened $F(\nu)$ in erg cm^{-2} s^{-1} Hz^{-1} is calculated from the flux density $F(\nu)$ (results are given in Table 1).

3. Preliminary Model of the System

3.1. Stellar Model

Kjurkchieva et al. (2017) reported preliminary models for the low and high states of J1621. They failed to obtain an acceptable solution using the *PHOEBE* code for the AAVSO V filter light curve during the outburst or for their BRI filters light curves taken shortly after J1612 had returned to its low state. The photometric data we report here are of higher S/N, are more numerous, and were taken in BVRI filters. Observations covering the entire orbital period were phased with the ephemeris: $T_0 = 2{,}457{,}552.41130\,(\pm 0.00034) + 0.207852\,\mathrm{P}$, where the zero epoch corresponding to the minimum, which was deeper at outburst, was derived from our new observations. We made no attempt to correct the period of the system, as phasing of our observations with the above period value (taken from Kjurkchieva et al. 2017) showed no noticable phase shift. Furthermore, we kept the phase shift as a free parameter that accounts for the innacuracy of the assumed period in the ephemeris. As a first step, we looked for the best possible solution of the light curve in the low state. We analyzed the light curves taken in 2016 August, more than two months after the outburst. For this purpose, we applied a modified Wilson–Devinney code and its improvements (W–D; Wilson &

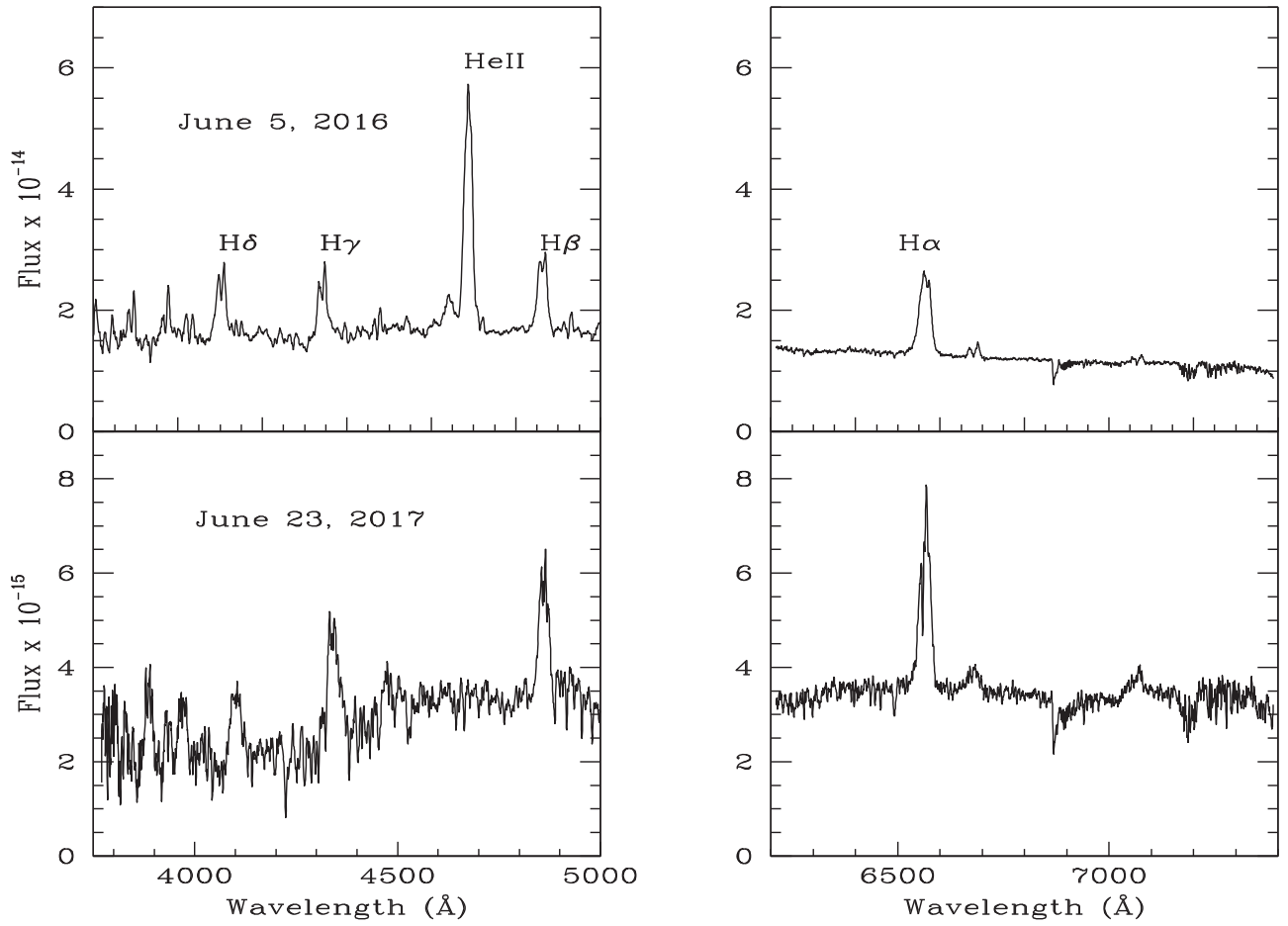

Figure 6. Comparison of spectra taken at outburst (top panels) and at quiescence (bottom panels). The blue part is shown on the left while the H_α region is shown on the right. The most prominent lines are labeled in the top panels.

Table 1
Summary of the *Swift* UVOT Observations of 2MASS J16211735+4412541

Date	UT	Band	Exp. (s)	Mag	dereddened Mag	$F(\nu)$	$\log_{10}\nu$
2016.06.10	10:24:56	UVW2	75.939	16.05	15.97 ± 0.09	$(3.01 \pm 0.24) \times 10^{-27}$	15.169
2016.06.10	10:31:55	UVM2	1283.49	16.07	15.99 ± 0.04	$(3.10 \pm 0.12) \times 10^{-27}$	15.129
2016.06.10	10:17:29	UVW1	75.946	16.12	16.06 ± 0.09	$(3.35 \pm 0.26) \times 10^{-27}$	15.063
2016.06.10	10:19:57	U	75.9439	15.42	15.38 ± 0.04	$(1.02 \pm 0.04) \times 10^{-26}$	14.933
2016.06.10	10:27:24	V	75.9438	15.05	15.02 ± 0.04	$(3.56 \pm 0.14) \times 10^{-26}$	14.744
2016.06.10	10:22:26	B	76.0405	15.62	15.58 ± 0.04	$(2.36 \pm 0.08) \times 10^{-26}$	14.840
2016.06.14	19:51:40	UVW2	147.305	17.43	17.35 ± 0.10	$(8.50 \pm 0.80) \times 10^{-28}$	15.169
2016.06.14	19:59:17	UVM2	147.311	17.68	17.60 ± 0.15	$(7.00 \pm 1.00) \times 10^{-28}$	15.129
2016.06.14	20:03:07	UVW1	147.312	17.01	16.95 ± 0.09	$(1.48 \pm 0.12) \times 10^{-27}$	15.063
2016.06.14	20:06:55	U	115.704	16.32	16.28 ± 0.05	$(4.45 \pm 0.22) \times 10^{-27}$	14.933
2016.06.14	19:55:28	V	147.312	15.21	15.18 ± 0.04	$(3.08 \pm 0.12) \times 10^{-26}$	14.744
2017.01.13	01:35:52	UVW2	477.292	17.81	17.73 ± 0.08	$(5.96 \pm 0.42) \times 10^{-28}$	15.169
2017.01.16	18:39:48	UVW2	541.186	17.46	17.38 ± 0.07	$(8.22 \pm 0.51) \times 10^{-28}$	15.169
2017.01.19	11:49:10	UVW2	519.371	17.76	17.68 ± 0.08	$(6.24 \pm 0.44) \times 10^{-28}$	15.169

Note. $F\nu$ given in units of erg cm^{-2} s^{-1} Hz^{-1}.

Devinney 1971; Wilson 1979; Wilson et al. 2010; Wilson & Van Hamme 2014; Zola et al. 2017), appended with the Monte Carlo search algorithm. Computations were done with mean points, about 110 of them in each filter. We made the following assumptions: the temperature of the secondary, which we assume to fill its Roche lobe, was set to 4300 K, which is appropriate for a dwarf of mid-K spectral type. The mass ratio was also fixed at the value of $q = 0.45$ (following Thorstensen 2016), and the albedo and gravity darkening coefficients were set to their theoretical values. For the low temperature secondary with a convective envelope, the albedo and the gravity darkening coefficients were set to 0.5 and 0.32, respectively, while for the primary both were set to 1.0. Limb darkening coefficients were taken from the Claret et al. (2012, 2013) tables. The Monte Carlo search method does not require initial parameters; the search is done in the set

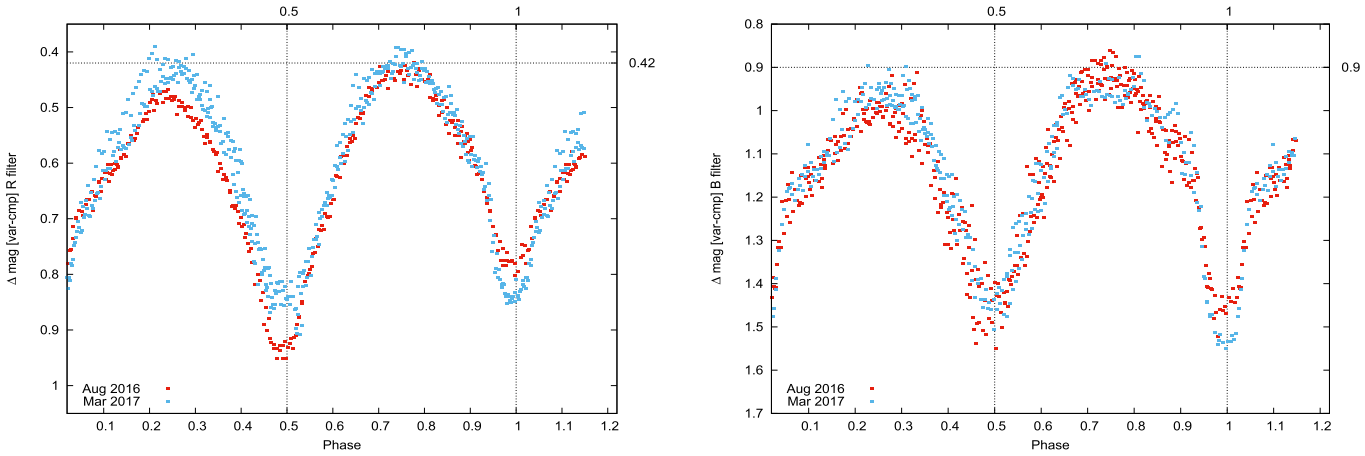

Figure 7. Evolution of the light curve between 2016 August and 2017 March. The light curves taken in the R filter are shown in the left panel, while those observed through the B filter are shown in the right one.

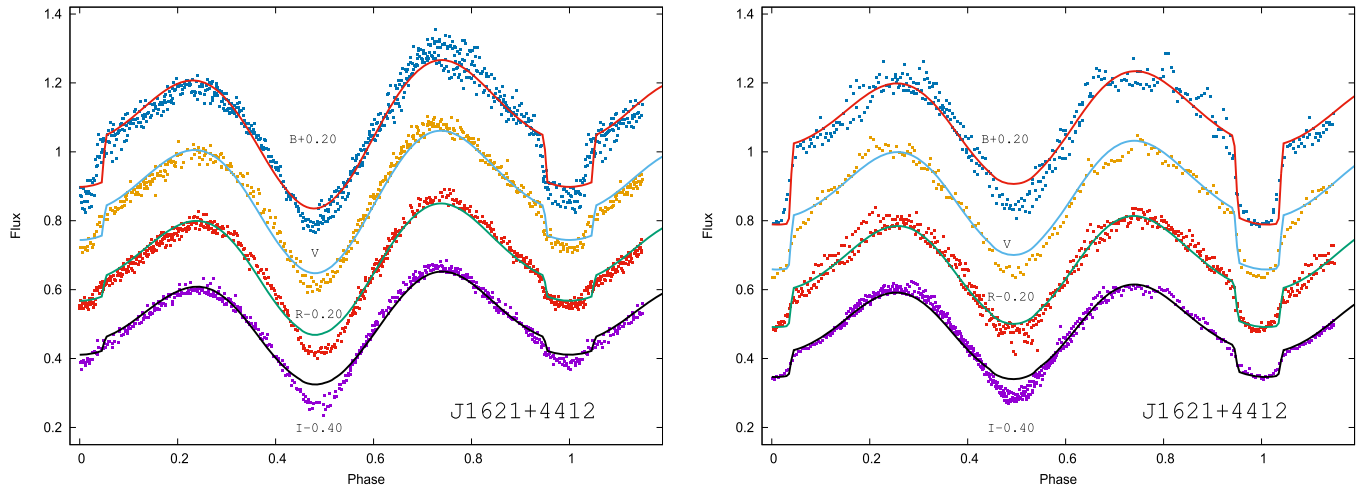

Figure 8. Best fit obtained within the W–D model (IPB = 0 only). The left panel shows data taken in 2016 August, while the right panel shows data taken in 2017 March. Observations are plotted by dots, while continuous lines represent the model.

ranges of free parameters: orbital inclination, the primary component temperature, and its potential, as well as the luminosity of the primary. To account for different maxima heights, a cool spot was also included in the model. Initially, with the observed spectroscopic signature, we assumed that the difference in heights was solely due to a hot spot. However, comparison of the light curves taken in quiescence revealed that the system did not change its brightness at the second maximum (higher in 2016 August) in 2017 March (see Figure 7). This is clearly seen in the left panel in Figure 7 (showing the light curve in the R filter), while the panel on the right (the light curve in the B filter) shows evidence that a hot spot also influences the shape.

Instead, in 2017 March, the system at the first quadrature is brighter, indicating that apart from the presence of a hot spot, the dominant effect is due to a cool spot(s), likely present on the secondary star. Since we placed the spot on the equator of the secondary, the spot introduced an additional three free parameters: its location in longitude, temperature factor, and size. We searched the entire equator for the spot location. Furthermore, we performed our computations with the parameter IPB = 0, which is the normal usage of the W–D code. With IPB set to 0 the program computes the luminosity of the secondary component from temperatures T_1 and T_2, the luminosity of the primary star, the radiation laws and the system geometry. Further details about controlling the W–D code with this and other parameters can be found in the program manual and documentation, which is available online.[10] The best fit that can be obtained under these assumptions to the 2016 August data set is shown in the left panel of Figure 8.

This model does reproduce the overall shape of the observed light curves everywhere except during the secondary minimum and the discrepancy grows toward longer wavelengths. Also, the primary minimum is somewhat too shallow in B and I filters (left panel in Figure 8). What can be inferred from this exercise is that the object that obscures the companion in the secondary minimum must be larger and does not radiate as a normal star. To confirm the latter, we performed additional computations, this time with the control parameter IPB set to 1. This decouples the component's luminosities and they both can be adjusted. With this setup, we derived an improved fit, still not perfect, but we were able to match the depth of the secondary minimum closely and improve the fit in the primary one. However, the shape of the secondary eclipse is different than that observed.

[10] ftp://ftp.astro.ufl.edu/pub/wilson/

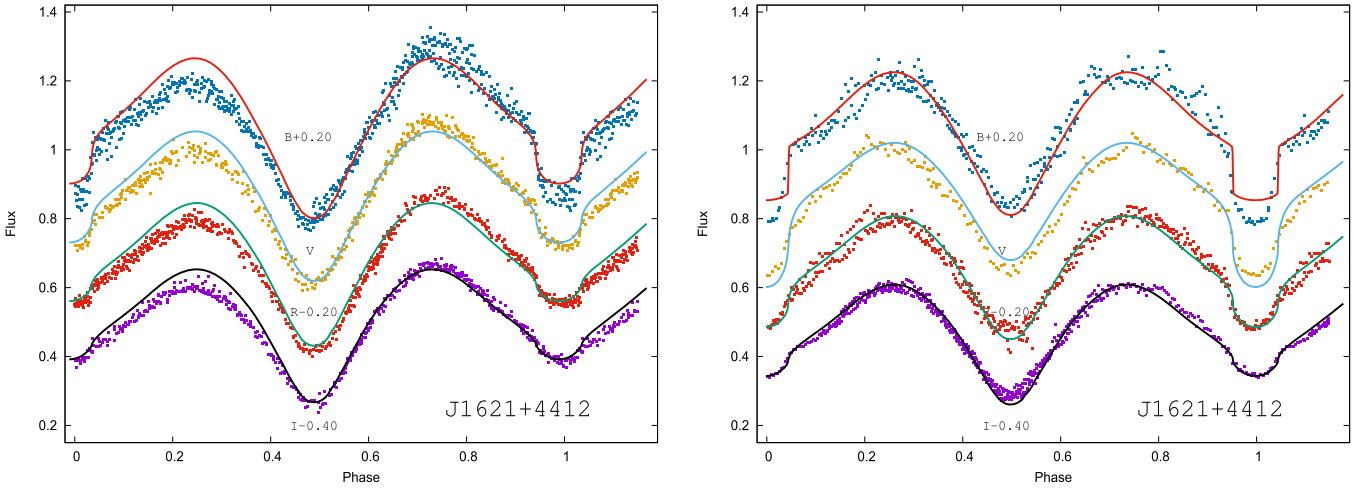

Figure 9. Best fit obtained within the circular disk model (top left) for the mass ratio fixed at $q = 0.45$. The observed points between phase 0.15 and 0.4 were discarded in computations (see the text for an explanation).

The stellar fits resulted in high inclination models. When IPB = 0, the best fit for post-outburst data taken in 2017 August was obtained for $i = 86°$, $T_1 = 8500$ K, and the fractional radius of the primary component $r_{\rm side} = 0.027$ (in orbital separation units). For IPB = 1, we arrived at an even higher inclination of $i = 89.^{\circ}7$ and a large primary with the $r_{\rm side} = 0.12$. In this case, the temperature of the primary cannot be reliably estimated. We repeated the computations for the more recent, 2017 March data, and we obtained a qualitatively very similar result (though the resulting numbers were somewhat different: e.g., $i = 84°$ and $T_1 = 8470$ K for the IPB = 0 solution). The fit is also presented in Figure 8 (right panel). Our computations done with the W–D code indicate that the light curve of J1621 cannot be reproduced with a stellar model alone. When the luminosities of the stars are coupled (IPB = 0) one cannot fit the proper depths of both minima. Our results (and those of Kjurkchieva et al. 2017) indicate that the primary does not radiate as a typical star. We conclude that an accretion disk must be added into the model for the right reconstruction of the entire light curve.

3.2. Disk Model in Quiescence

Our next trial was done with a simple, phenomenological disk model. We added a circular, optically thick disk surrounding the primary component. The disk temperature distribution was assumed for the stationary accretion case. The disk vertical thickness grows linearly with its radius. Radiation from stars is computed in the same way as the W–D code does, but additional effects arising due to the disk presence are accounted for: the obscuration (partial or total, depending on the orbital inclination and the outer disk thickness) of the primary, eclipse of the secondary, mass donor star by the disk and self-obscuration of the disk. Also, for this model, the search was done with the Monte Carlo method. Further details about the model can be found in Zola (1991, 1992). The code does not include the presence of a hot spot; therefore, we discarded data between phases 0.6 and 0.9 in the modeling both in the 2016 August and 2017 March data. For the latter, the difference between maxima was much less pronounced than for the post-outburst, 2016 August observations. The usage of such a phenomenological model requires imposing as many constraints as possible. We made similar assumptions to those applied in the W–D computations concerning the secondary temperature and the system mass ratio. Additionally, we assumed that the primary is a white dwarf and estimated its potential at 150, corresponding to a fractional radius of about 0.005 (in component separation units). Furthermore, the disk outer temperature was arbitrarily set to 7000 K, and the temperature distribution was assumed as that for stationary accretion. Based on these quantities, as well as the above mentioned white dwarf parameters, the vertical structure of the accretion disk was computed, resulting in a very thin geometrical disk thickness. With this result, we also fixed the disk thickness parameter at $0.^{\circ}5$.

Computations were performed separately for the 2016 August and 2017 March quiescent data. The following parameters were treated as free: orbital inclination, the luminosity of the primary as well as the accretion disk radius (r_d) and its luminosity (l_d), that has a similar meaning as the third light parameter (l_3) in the W–D code. Therefore, it cannot be directly compared with the input luminosities of stellar components L_1 and L_2. However, unlike the l_3 which is assumed to be constant throughout the entire orbital period, l_d can vary, if the accretion disk is eclipsed or its shape is asymmetrical. After achieving convergence, a somewhat different orbital inclination was derived for the two sets. For the final step, a mean inclination value was calculated and modeling was redone with this parameter fixed. The best fit obtained for the circular disk model is graphically presented in Figure 9 (2016 August observations are shown in the left panel, while those from 2017 March are in the right panel). The different shape of the J1621 light curve, the near disappearance of the maxima difference, and especially the deeper primary minimum, cannot be described well with the same parameters as those used for the 2016 August data, for which the model resembles the observations reasonably well. There remains only an asymmetry of the secondary minimum in the B filter and a bit larger depth in the I filter. For the 2017 March data, the trend is much more noticeable: the model predicts a secondary minimum that is too deep in R and I filters, while the primary is too shallow in B and V.

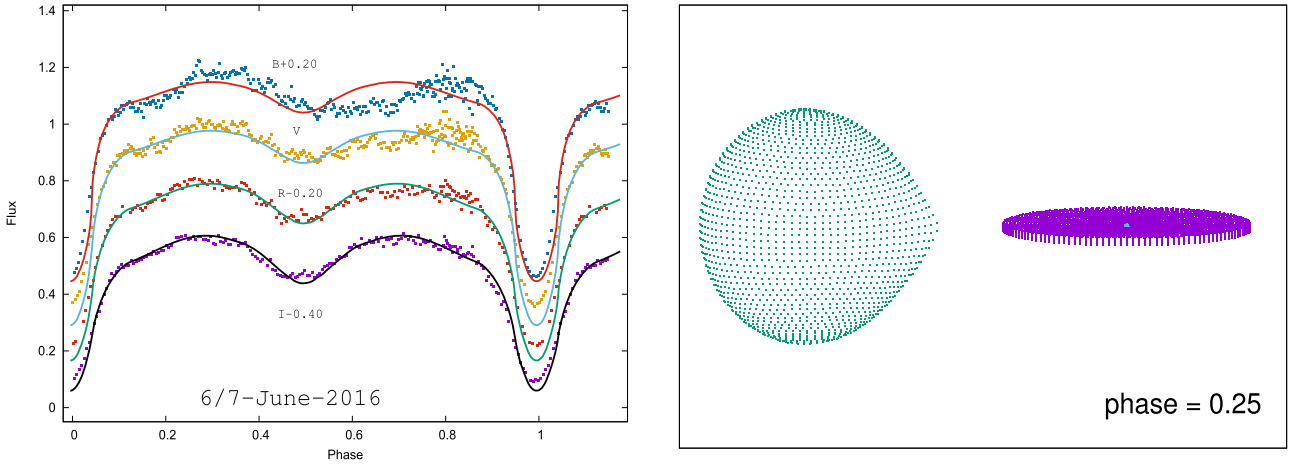

Figure 10. Best fit to observations at outburst obtained within the circular disk model (left) and a view of the J1621 model at phase 0.25 (right panel).

3.3. Disk Model in Outburst

The next attempt of our preliminary modeling was applied to the light curve at outburst. Only on June 6/7 does the light curve of J1621 not exhibit a significant difference between the maxima heights. However, it shows severe distortions, especially in the B filter. We applied the disk model and performed the fitting with the same assumptions as for the computations done for the quiescent light curves, but increased the outer disk temperature to 1000 K and also arbitrarily increased its thickness three times to 1.°5. With inclination, the mass ratio, disk outer temperature and thickness fixed, we derived a reasonable fit to the observed light curves. The secondary minimum depth and widths are closely matched; however, the depth of the primary minimum in our model is somewhat deeper in V, R, and I filters than the observed one.

Our best fit arrived at a solution with a disk at the maximum size allowed (that of the side radius of the Roche lobe). The disk light is dominant in all filters but I, its contribution to the total system light reaches 54% in the B, 58% in V, 51% in R, and 44% in I filters. The theoretical lines plotted on the observations are shown in the left panel of Figure 10. We show a view of the model in the right panel of the same figure. The system parameters derived within the disk models are presented in Table 2. In this table, we also included the values of the limb darkening (x_1, x_2) coefficients that were chosen by the code for the temperatures corresponding to final solutions.

Table 2
Parameters Derived for J1621 within the Disk Models

Parameter	2015 June 6	2016 August	2017 March
i[a,b]	84.°3	84.°3	84.°3
T_1	46,810 ± 2,200 K	18,790 ± 2,300 K	26,220 ± 2,430 K
T_2[a]	4,300 K	4,300 K	4,300 K
Ω_1[a]	150	150	150
Ω_2[b]	2.7784	2.7784	2.7784
q[a]	0.45	0.45	0.45
r_d	0.387 ± 0.090	0.452 ± 0.047	0.430 ± 0.045
Td_{out}	10,000 K	5000 K	5000 K
β[b]	1.°5	0.°5	0.°5
L_1 (B)	2.032 ± 0.603	2.313 ± 0.479	3.010 ± 0.563
L_1 (V)	0.900 ± 0.391	1.047 ± 0.216	1.155 ± 0.232
L_1 (R)	0.623 ± 0.208	0.624 ± 0.109	0.742 ± 0.107
L_1 (I)	0.325 ± 0.088	0.283 ± 0.044	0.344 ± 0.046
L_2 (B)[b]	3.315	10.884	10.168
L_2 (V)[b]	3.779	11.143	9.138
L_2 (R)[b]	4.879	11.465	10.325
L_2(I)[b]	6.172	11.617	10.965
l_d (B)	0.542 ± 0.110	0.036 ± 0.048	0.017 ± 0.096
l_d (V)	0.584 ± 0.160	0.068 ± 0.054	0.191 ± 0.083
l_d (R)	0.514 ± 0.146	0.055 ± 0.040	0.099 ± 0.037
l_d (I)	0.440 ± 0.146	0.068 ± 0.037	0.069 ± 0.030
x_1 (B)[b]	0.221	0.444	0.354
x_1 (V)[b]	0.195	0.388	0.314
x_1 (R)[b]	0.172	0.331	0.273
x_1 (I)[b]	0.135	0.248	0.218
x_2 (B)[b]	0.909	0.909	0.909
x_2 (V)[b]	0.826	0.826	0.826
x_2 (R)[b]	0.755	0.755	0.755
x_2 (I)[b]	0.618	0.618	0.618

Notes. On June 6th, the system was in outburst, while 2016 August and 2017 March models represent the quiescent phase. L_1 and L_2 represent the W–D model input luminosities. Errors of adjusted parameters are given at the 90% confidence level.
[a] Fixed.
[b] Computed.

4. Summary of Results and Conclusions

A model containing only stars cannot fit the light curve of J1621 well in its low state. Also, the fits in terms of the weighted reduced χ^2 values are worse compared to the disk models: 19.83 versus 9.21 for the 2016 August data, for the stellar and disk models, respectively, and, 17.21 versus 14.80 for the 2016 March observations. Taking into account the results from Section 3.1, we argue that the primary is not a normal star but a highly flattened object likely consisting of a WD surrounded by an accretion disk. Our preliminary computations indicate that the accretion disk is present in the system both during the outburst and in the post-outburst phase, confirmed by the presence of doubled Balmer emission lines during both states, as well as the flickering seen in optical wavelengths and the secondary minimum that is too deep. J1621 appears to be very similar to the high inclination dwarf nova IP Peg at outburst, with both showing abnormally strong He II fluxes.

Within a phenomenological disk model with several constraints imposed, we were able to obtain a reasonable fit of the J1621 light-curve shape as seen in 2016 August while discarding phases between 0.15 and 0.4, as the code does not

account for the presence of spots in a system. The fit to the 2017 March data that show a deeper primary minimum is worse. Most noticeably, we could not match the right depths of the primary minimum both in B and V filters. The depth of the secondary also does not correctly resemble the observed one. We believe that the most likely reason could be changing disk parameters, including the temperature distribution along the disk surface that was fixed to the stationary accretion case, but also the assumption that the disk is optically thick can be wrong. The changing values for the K semi-amplitude between outburst and quiescence corroborate significant disk changes. Finally, the mass ratio used in our preliminary modeling that was estimated from the Balmer emission lines, may be subject to uncertainty and could be another reason for the discrepancy between the models and observations although our value of 0.45 is similar to that of IP Peg. Our attempts of including the system mass ratio as a free parameter resulted in significantly different mass ratio values for the two quiescent sets of data and we consider them to be unreliable.

The modeling must be done with a more physical disk model, e.g., accounting for the disk to be partly transparent at quiescence, or the presence of a hot spot on the accretion disk rim, as well as a cool spot(s) on the mass losing star. A final model would also require reliable values for the secondary temperature and the system mass ratio.

The most likely cause of the outbursts is a disk instability, when the mass transfer leads to a buildup of the disk, resulting in a dwarf nova outburst as the viscosity and accretion rate throughout the disk increases (Warner 1995). This would cause the disk to brighten and possibly to increase its radius (and thickness). The presence of a cool spot on the secondary component soon after the outburst, and its disappearance in less than a year after, may indicate that an enhanced magnetic activity might have triggered the outburst. The object seems to resemble HD 109962 (V1129 Cen), which exhibits similar spectroscopic features and outbursts occurring about once a year and lasting about 40 days (Walter et al. 2006). However, the duration of the current outburst in J1621 is shorter (10+ days) and the frequency of outbursts is currently uncertain. The archival data show a brightening of the system to a similar level on 2006 August 4th (Kjurkchieva et al. 2017). *GALEX* (Martin et al. 2005) took UV measurements just before that date, on 2006 July 26th. Observations in the *Swift* W2 filter made right after the 2016 outburst show J1621 to be almost 3 mags brighter than the *GALEX* magnitude in the NUV filter that has a similar effective wavelength and transparency window as W2. Most likely, the WD was still hot as detected by *Swift* shortly after the outburst, while *GALEX* observed it at its quiescent cool state, just a week before the outburst in 2006. The X-ray flux as well as the UV colors of the recent *Swift* observations are typical of a dwarf nova binary.

The EW-type light curve at quiescence gives an impression of a contact/near-contact binary at red wavelengths. The light curves in blue bands still exhibit a trace of an almost flat bottom primary minimum with depth increasing toward shorter wavelengths 8 months after the outburst. Its depth was measured to be larger in 2017 March than in July and 2016 August (see Figures 8 and 9). It remains to be seen if this feature disappears with time, as the white dwarf cools to its quiescent level, and indeed a light curve typical of a near-contact or a contact system will be observed. Our results show that a fraction of contact systems, especially those classified on the basis of light curves provided by the large surveys, may be cataclysmic systems.

We gratefully acknowledge support through the NCN 2012/07/B/ST9/04432 grant. P.S. acknowledges support from NSF grant AST 1514737. Some of the data presented in this paper were obtained from the Barbara A. Mikulski Achive for Space Telescopes at the Space Telescope Science Institute (MAST). STScI is operated by the Association of Universities for Research in Astronomy, Inc., under NASA contract NAS5-26555. The MAST for non-*HST* data is supported by the NASA Office of Space Science via grant NAG5-7584 and other grants and contracts.

ORCID iDs

S. Zola https://orcid.org/0000-0003-3609-382X
P. Szkody https://orcid.org/0000-0003-4373-7777
B. Debski https://orcid.org/0000-0002-2050-9133
D. Reichart https://orcid.org/0000-0002-5060-3673

References

Breeveld, A. A., Landsman, W., Holland, S. T., et al. 2011, in AIP Conf. Ser. 1358, ed. J. E. McEnery, J. L. Racusin, & N. Gehrels (Melville, NY: AIP), 373
Burrows, D. N., Hill, J. E., Nousek, J. A., et al. 2005, SSRv, 120, 165
Claret, A., Hauschildt, P. H., & Witte, S. 2012, A&A, 546, A14
Claret, A., Hauschildt, P. H., & Witte, S. 2013, A&A, 552, A16
Drake, A. J., Djorgovski, S. G., Mahabal, A. A., et al. 2016, ATel, 9112, 1
Drake, A. J., Gänsicke, B. T., Djorgovski, S. G., et al. 2014a, MNRAS, 441, 1186
Drake, A. J., Graham, M. J., Djorgovski, S. G., et al. 2014b, ApJS, 213, 9
Fitzpatrick, E. L. 1999, PASP, 111, 63
Kalberla, P. M. W., Burton, W. B., Hartmann, D., et al. 2005, A&A, 440, 775
Kjurkchieva, D. P., Popov, V. A., Vasileva, D. L., & Petrov, N. I. 2017, NewA, 52, 8
Lohr, M. E., Norton, A. J., Kolb, U. C., et al. 2013, A&A, 549, A86
Maehara, H. 2016, ATel, 9113, 1
Marsh, T. R., & Horne, K. 1990, ApJ, 349, 593
Martin, D. C., Fanson, J., Schiminovich, D., et al. 2005, ApJL, 619, L1
Palaversa, L., Ivezić, Ž, Eyer, L., et al. 2013, AJ, 146, 101
Piche, F., & Szkody, P. 1989, AJ, 98, 2225
Roming, P. W. A., Kennedy, T. E., Mason, K. O., et al. 2005, SSRv, 120, 95
Schlafly, E. F., & Finkbeiner, D. P. 2011, ApJ, 737, 103
Schlegel, D. J., Finkbeiner, D. P., & Davis, M. 1998, ApJ, 500, 525
Steeghs, D., Horne, K., Marsh, T. R., & Donati, J. F. 1996, MNRAS, 281, 626
Thorstensen, J. 2016, ATel, 9141, 1
Tylenda, R., Hajduk, M., Kamiński, T., et al. 2011, A&A, 528, A114
Walter, F., Bond, H. E., Pasten, A., & Otero, S. 2006, IAU Circ., 8663, 1
Warner, B. 1995, CAS, 28
Wilson, R. E. 1979, ApJ, 234, 1054
Wilson, R. E., & Devinney, E. J. 1971, ApJ, 166, 605
Wilson, R. E., & Van Hamme, W. 2014, ApJ, 780, 151
Wilson, R. E., Van Hamme, W., & Terrell, D. 2010, ApJ, 723, 1469
York, D. G., Adelman, J., Anderson, J. E., Jr., et al. 2000, AJ, 120, 1579
Zejda, M., & Pejcha, O. 2016, ATel, 9132, 1
Zola, S. 1991, AcA, 41, 213
Zola, S. 1992, AcA, 42, 355
Zola, S. 1995, A&A, 294, 525
Zola, S. 1998, AcA, 48, 373
Zola, S., Baran, A., Debski, B., & Jableka, D. 2017, MNRAS, 466, 2488